

Multicellularity and the functional interdependence of motility and molecular transport

Cristian A. Solari*, Sujoy Ganguly†, John O. Kessler†, Richard E. Michod*, and Raymond E. Goldstein†*§¶

Departments of *Ecology and Evolutionary Biology and †Physics, ‡Program in Applied Mathematics, and §BIO5 Institute, University of Arizona, Tucson, AZ 85721

Edited by Robert H. Austin, Princeton University, Princeton, NJ, and approved December 4, 2005 (received for review May 7, 2005)

Benefits, costs, and requirements accompany the transition from motile totipotent unicellular organisms to multicellular organisms having cells specialized into reproductive (germ) and vegetative (sterile soma) functions such as motility. In flagellated colonial organisms such as the volvoclean green algae, organized beating by the somatic cells' flagella yields propulsion important in phototaxis and chemotaxis. It has not been generally appreciated that for the larger colonies flagellar stirring of boundary layers and remote transport are fundamental for maintaining a sufficient rate of metabolite turnover, one not attainable by diffusive transport alone. Here, we describe experiments that quantify the role of advective dynamics in enhancing productivity in germ somadifferentiated colonies. First, experiments with suspended deflagellated colonies of *Volvox carteri* show that forced advection improves productivity. Second, particle imaging velocimetry of fluid motion around colonies immobilized by micropipette aspiration reveals flow fields with very large characteristic velocities U extending to length scales exceeding the colony radius R . For a typical metabolite diffusion constant D , the associated Peclet number $Pe = 2UR/D \gg 1$, indicative of the dominance of advection over diffusion, with striking augmentation at the cell division stage. Near the colony surface, flows generated by flagella can be chaotic, exhibiting mixing due to stretching and folding. These results imply that hydrodynamic transport external to colonies provides a crucial boundary condition, a source for supplying internal diffusional dynamics.

diffusion | flagella | *Volvox*

The efficient exchange of nutrients, metabolites, and wastes is among the most basic factors affecting the fitness of organisms. Understanding the effect of resource delivery and exchange on metabolic rate, as organisms increase in size, is leading to rapid advances across disparate fields of the life sciences, from comparative biology to ecosystem ecology (1–4). Yet, these insights have not been applied to the analysis of the evolutionary transitions which underlie the hierarchy of life (5, 6). Although cooperative endeavors provide substantial benefits, certain key problems must be solved for a group to emerge into a new complex individual. As lower level units (cells) associate to form groups, the constraints of surface to volume ratio, S/V , and of spatial organization limit the type and extent of interactions with the environment, with profound effects on metabolism, growth rate, viability, and fecundity. We refer to this as the “transport limitation” and view it as a general aspect of evolutionary transitions in individuality.

Nutrient consumption increases proportionally with the size of the organism, creating an increased boundary layer of nutrient depletion. In the absence of active mixing of the medium, this decreases the passive diffusion of nutrients. This transport limitation constraint as size increases can be circumvented in several ways. For example, depending on the geometry, increasing in size may not decrease the S/V ratio; e.g., a cylindrical organism can indefinitely increase in volume without decreasing S/V if its radius r remains constant, for then $S/V = 2/r$ (7). Also, some organisms live in environments that favor the active mixing

of nutrients through laminar or turbulent flows (e.g., a sessile organism in a flowing current). There are even unicells that are able to reach the sizes of small multicellular organisms by having specific geometries and living in specific favorable environments (8). We focus here on the lineages that we hypothesize were able to evolve large multicellular forms by actively mixing the surrounding fluid with self-generated flagellar-driven flows.

Using as model organisms the volvoclean green algae (class: Chlorophyceae) (9), we study here the biological significance of collective modes of hydrodynamic transport. These aquatic flagellated organisms (Fig. 1) range from unicellular organisms such as *Chlamydomonas reinhardtii* to colonies made of 4–64 cells with no cell differentiation (e.g., *Gonium*, *Eudorina*), to multicellular individuals (e.g., *Volvox*) composed of 1,000–50,000 differentiated cells (9–11). Specialization into reproductive (germ cells) and vegetative (sterile flagellated cells) functions, termed “germ-soma separation,” characterizes the large members. The number of somatic cells per reproductive cell (S/R ratio) increases with colony size (10). *Volvox* species with germ-soma separation are not monophyletic. These complex forms have evolved several times independently, from quite different ancestors (11, 12). Supporting this ease of evolutionary transition in Volvocales is the underlying genetic architecture responsible for the separation of germ and soma, which does not involve many genetic steps (9). Note that the number of cells in Volvocales is determined by the number of cleavage divisions that take place during embryonic development. Cell number is not augmented by accretory cell divisions after juveniles hatch (13).

Because the Volvocales are denser than water, they need motility to avoid sinking and to reach light and nutrients (14). Undifferentiated colonies face motility problems even at a small size (e.g., 32-cell colonies, *Eudorina*; Fig. 1) as a result of the “flagellation constraint” [motility is inhibited during cell division (10)]. Nonetheless, even in the absence of this constraint, larger colonies would sink if they did not increase their flagellar swimming force by investing in somatic cells and the associated extracellular matrix (ECM). This need arises from the enlargement of reproductive cells, which increases the mean density of the colony (15). We argue here that this investment in somatic cells for motility has the additional and important benefit of enhanced molecular transport of nutrients and wastes thanks to the flow created by collective flagellar beating.

Evidence for the importance of flagella- and cilia-driven flows in eukaryotes is provided by the high degree of sequence conservation between flagellar proteins of unicellular organisms such as *C. reinhardtii* and ciliary proteins of multicellular organisms such as mammals (16, 17). Moreover, it is becoming increasingly clear from a range of recent studies that these flows

Conflict of interest statement: No conflicts declared.

This paper was submitted directly (Track II) to the PNAS office.

Abbreviations: ECM, extracellular matrix; PIV, particle imaging velocimetry.

¶To whom correspondence should be addressed. E-mail: gold@physics.arizona.edu.

© 2006 by The National Academy of Sciences of the USA

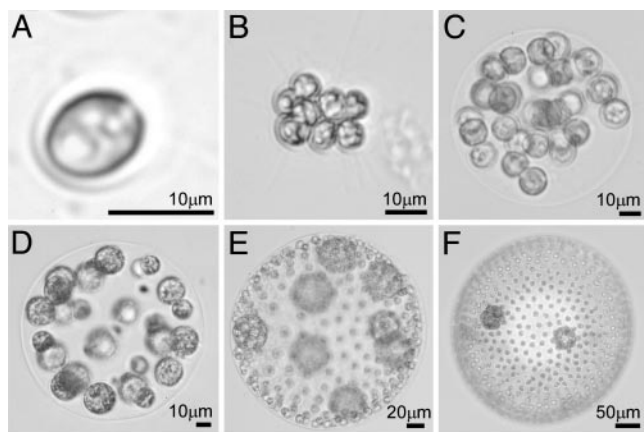


Fig. 1. Species of volvoclean green algae spanning a large range in size. Shown are the single-cell *C. reinhardtii* (A), undifferentiated colonies *Gonium pectorale* (8 cells) (B) and *Eudorina elegans* (32 cells) (C), and those with germ-soma differentiation *Pleodorina californica* (64 cells) (D), *V. carteri* ($\approx 1,000$ cells) (E), and *Volvox aureus* ($\approx 2,000$ cells) (F).

can play a central role in multicellular systems, broadly interpreted. Examples include morphogenetic symmetry-breaking driven by ciliary flows (18, 19), microfluidic devices that might use bacterial carpets (20), self-concentration of chemotactic bacteria (21, 22), and large-scale coherence in concentrated suspensions (21, 23). Common to all are (i) fluid velocities reaching hundreds of microns per second and (ii) coherent motion with length scales extending over very many cells, exceeding hundreds of microns. Because the diffusion constant D of modest size solutes (a chemical messenger or a metabolite) is at most 10^{-6} to 10^{-5} cm^2/s , advection in flows with the above characteristics can easily dominate diffusion. Let us recall that if a molecular solute of concentration C exhibits transport by diffusion and advection, and \mathbf{u} is the local fluid velocity, then

$$C_t + \mathbf{u} \cdot \nabla C = D \nabla^2 C. \quad [1]$$

If U is a characteristic fluid velocity varying on a length scale L , then $\mathbf{u} \cdot \nabla C \sim UC/L$ and $D \nabla^2 C \sim DC/L^2$. The ratio of these advective and diffusive terms, or equivalently the ratio of the diffusion time L^2/D to the advective time L/U , then defines the Peclet number (24),

$$Pe = \frac{UL}{D}. \quad [2]$$

If $Pe < 1$, diffusion outcompetes transport by advection from the flowing medium, whereas if $Pe > 1$, advection dominates. When L is the size of a bacterium ($\approx 10^{-4}$ cm) and U is a swimming speed ($\approx 10^{-3}$ cm/s), then $Pe \sim 10^{-2}$ to 10^{-1} for small solutes. Advection is therefore negligible (25) and may be ignored in dynamic models of chemotaxis and chemical signaling (26). The situation changes radically when U and L are as large as found in the systems described above, where many closely spaced moving entities (motile bacteria or cilia) collectively generate flows. Then $Pe \sim 10^2$ and advection can not be neglected. Such flows may also exhibit long correlation lengths and times and can be chaotic, as seen even at the single cell level (27), exhibiting stretching and folding that enhance local mixing.

It has been argued that larger differentiated Volvocales with high S/R ratios are efficient in nutrient uptake and storage, especially in eutrophic conditions. This “source-sink” hypothesis (28, 29), in which soma is the source and germ the sink, implies that in large colonies the division of labor prevents the inhibition of nutrient uptake by previously acquired resources (following

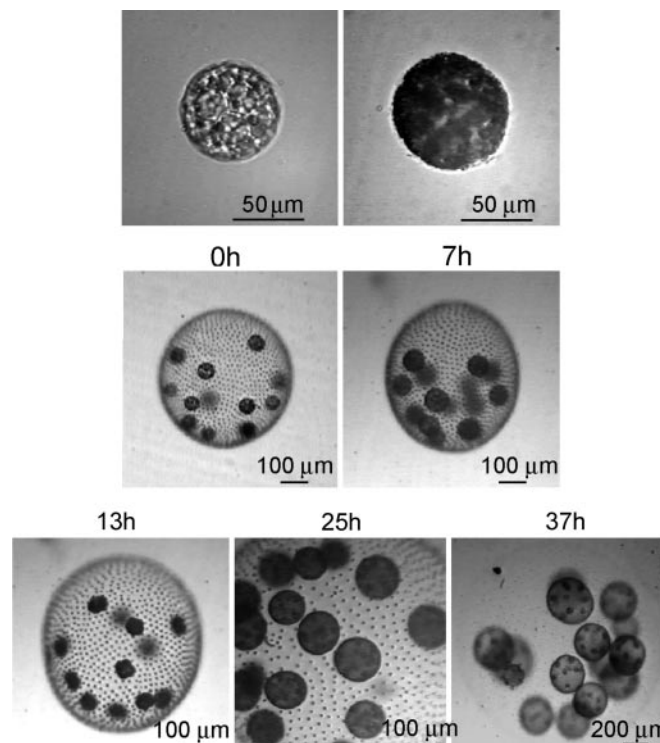


Fig. 2. The asexual life cycle of *V. carteri* when synchronized in a 16 h light/8 h dark cycle. 0h (upper), a germ cell from newly hatched colonies; 0h (lower), a newly hatched colony (2 h into the light cycle); 7h (upper), a germ cell reaching the end of its growth phase and ready to start cleavage; 7h (lower), a colony 7 h after having hatched; 13h, 1 h before the end of the light cycle (germ cells are in the middle of their cleavage phase); 25h, 3 h into the next light cycle (in the dark cycle, germ cells finished cleavage and inverted, and now the daughter colonies are fully formed inside the mother colony); 37h, 1 h before the end of the light cycle (daughter colonies have been growing inside the mother colony). Hatching of daughter colonies takes place at the beginning of the next light cycle.

Michaelis–Menten kinetics). Tests of the source-sink hypothesis have not addressed the effect on nutrient uptake of the mixing driven by the flagella of somatic cells. Here, we specifically investigate the hypothesis that the apparatus that confers motility in large Volvocales also functions to enhance molecular transport, improving the acquisition of molecules important for productivity, and increasing the dispersal of waste products beyond the range of inadvertent diffusive recycling (7, 30). Using a combination of experimental methods, we provide quantitative evidence that collective flagellar beating in a species with germ-soma separation becomes important for enhancing colony growth. Also, we provide measurements of the collective fluid velocities driven by the flagella of the somatic cells at various stages in the life cycle. These results prove not only that the relevant Peclet numbers greatly exceed unity but also show intriguing variations during the life cycle. Taken together, these experimental results highlight a whole range of biologically significant factors in the hydrodynamics of flagellar-driven flows and, more universally, the physical constraints on the evolution of multicellularity.

Volvox carteri, the species used originally to test the source-sink hypothesis (28, 29), was chosen for our experiments because it is large enough to expect advection to have a significant effect on metabolite transport and hence colony growth. It is a colonial green alga formed by $\approx 1,000$ – $4,000$ mortal flagellated somatic cells and ≈ 8 – 16 immortal nonflagellated germ cells (9) (gonidia; Figs. 1 and 2). In *V. carteri*, the reproductive cells do not undergo

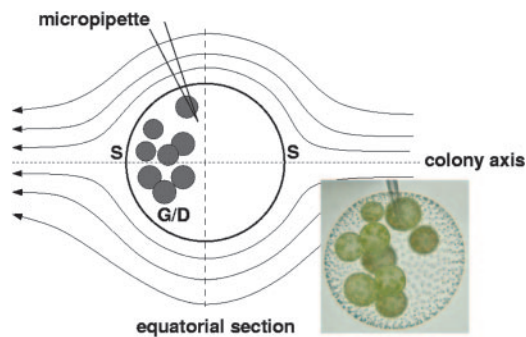


Fig. 3. Micropipette aspiration of *V. carteri* for PIV studies. Schematic shows streamlines symmetric about the colony axis, on which are located the two stagnation points (S). Germ cells/daughter colonies (G/D) are located in posterior half of colony. Dashed line indicates equatorial section of PIV flow field used to determine maximum fluid velocity.

binary fission; rather, each reproductive cell grows about 2^n -fold in size and then undergoes a rapid, synchronous series of n divisions (within the mother cell wall). This peculiar way of division, termed palintomy, is considered the ancestral developmental program in this group (13). The size a gonidium reaches before cleavage starts positively correlates with the size of the daughter colony it produces. Larger gonidia produce larger daughter colonies with higher number of cells (somatic and reproductive) (31). Thus, gonidia that reach a larger size before cleavage starts have higher fecundity.

Overview of Approaches and Results

To understand the effect of advection on colony productivity (fecundity), we measured the increase of the gonidium diameter in *V. carteri* during the growth phase, for a fixed time period before cleavage started. We compared the growth rate of *V. carteri* germ cells that were liberated by breaking the colonies apart, in deflagellated colonies, and in normal colonies. These gonidia, outside or inside colonies, were placed in either still or artificially mixed medium, with and without the presence of a flagellar regeneration inhibitor. Koufopanou and Bell (29) investigated the effects of isolating germ from soma. Our experiments generalize this work by consideration of the effects of fluid transport. We hypothesize that if advection driven by collective flagellar beating is important for nutrient uptake, then the growth rate of permanently deflagellated colonies placed in still medium ought to decrease. Under the same hypothesis, we expect this negative effect to disappear when those permanently deflagellated colonies are placed in a medium artificially mixed by air bubbling (“sparging”). Our results were in accord with these expectations. This effect is clearly due to modulation of nutrient uptake by advection or its absence. Thus, evidence shows that advection plays a significant role in the fitness of *V. carteri* colonies, likely by enhancing nutrient uptake.

The second part of our experimental program consists of direct measurements (Fig. 3) of fluid velocities driven by flagellar beating at various stages in *V. carteri*'s life cycle. These data yield the Peclet number and serve as benchmarks for a quantitative theory of nutrient uptake by these organisms. Combined, our results show that the flagellar transport/mixing effect is separate from the mechanisms underlying the source-sink hypothesis. We discuss implications that these effects may have on the emergence of multicellularity, accompanying cell differentiation in this lineage.

Results: Gonidia Growth

Table 1, which is published as supporting information on the PNAS web site, shows all of the parameter estimates with their

p values for the whole and reduced model from the additive multiple linear regression analysis. When colonies just hatched the average initial gonidia diameter was $46.81 \pm 0.76 \mu\text{m}$ for the still medium experiments and $52.25 \pm 0.92 \mu\text{m}$ for the sparged medium experiments ($n = 60$; S , Table 1). The latter experiments were performed 1 week later, continuing the use of the previously synchronized population. Thus, after 1 week, the average initial gonidia sizes from the same population synchronized under the same conditions were slightly larger. The two experiments were started with populations composed of different colony sizes. Small differences were also found between the two replicated experiments within the medium treatments ($R2$, S and $R2$, B , Table 1). Nevertheless, there was no significant difference in diameter increase between the gonidia in the still and sparged treatments (i.e., no interaction between the medium treatment and the final diameter; $\Delta d \times S$, Table 1) and between replicates within the medium treatments ($\Delta d \times R2$, S and $\Delta d \times R2$, B , whole model, Table 1). The average gonidium diameter increase in normal flagellated colonies was $12.92 \pm 0.90 \mu\text{m}$ in 7 h (Δd , Table 1; the average final germ cell diameter for the still and sparged experiments was $60.19 \pm 0.76 \mu\text{m}$ and $65.41 \pm 0.95 \mu\text{m}$, respectively; $n = 60$).

After correcting for variations between experiments, we found significant differences and interactions between the factors involved in the experiments (medium: still S or bubbling B , deflagellation D , broken colony L , and inhibitor I treatments). There is no evidence that transient deflagellation by itself decreases gonidium diameter growth, likely due to the rapid flagellar regeneration in the absence of the inhibitor (D , Table 1). In contrast, regardless of medium treatment, the gonidia from broken colonies grew on average $3.28 \pm 0.61 \mu\text{m}$ less in diameter than those from normal flagellated colonies (L , Table 1). The gonidia from colonies with the inhibitor treatment grew on average $1.57 \pm 0.58 \mu\text{m}$ less in diameter than those without the inhibitor (I , Table 1). These results were independent of the medium (no interaction between the deflagellation treatment, broken colony treatment, inhibitor, and medium; whole model $D \times S$, $L \times S$, and $I \times S$, Table 1).

After correcting for the negative effect of the inhibitor, we found an even larger decrease in the average gonidium diameter growth when permanently deflagellated colonies were placed in still medium [$-4.31 \pm 1.89 \mu\text{m}$; S : ($D \times I$), Table 1], i.e., an interaction between the deflagellation and inhibitor treatments. However, the negative effect disappeared when these colonies were placed in bubbling medium [B : ($D \times I$), Table 1]. Thus, permanently deflagellated colonies grew as well as normal flagellated colonies when the medium was artificially mixed! On the other hand, broken colonies behaved the opposite way, for when they were treated with the inhibitor and placed in still medium, there was no additional negative effect [no interaction between broken and inhibitor treatments; S : ($L \times I$), Table 1]. However, there was a significant decrease in germ cell diameter growth when broken colonies with the inhibitor treatment were placed in bubbling medium [$-4.73 \pm 1.90 \mu\text{m}$; B : ($L \times I$), Table 1]. These two negative effects are the largest in the analysis (Fig. 4).

In summary, we found that inhibiting advection by preventing collective flagellar beating decreases the growth rate of the gonidia within a colony. This negative effect disappears when the medium is artificially mixed, proving that the decrease in growth is due to the decrease in advection.

Because there was no difference in growth rates between colonies in sparged and still media when colonies were not permanently deflagellated, one infers that conditions in the still medium were optimum for the 7 h duration of experiments, and/or that flagellar mixing in the still medium was sufficient for allowing the same nutrient uptake as in the sparged medium. From the negative interaction between broken colonies and the

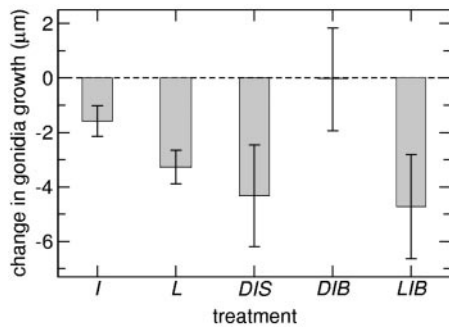


Fig. 4. Summary of germ cell growth experiments. Data show treatments that significantly affected the growth rate of germ cells compared with those of normal flagellated colonies in standard medium. *I*, inhibitor treatment; *L*, broken colonies treatment; *DIS*, deflagellated colonies with inhibitor in still medium; *DIB*, deflagellated colonies with inhibitor in bubbling medium; *LIS*, broken colonies with inhibitor in still medium; *LIB*, broken colonies with inhibitor in bubbling medium. *DIB* results illustrate the restoration of normal growth with artificial bubbling.

inhibitor, in the bubbling medium, one may infer that bubbling enhanced the absorption of the inhibitor by gonidia unprotected by the ECM. Because the results show that the inhibitor by itself only slightly affected growth (Table 1 and Fig. 3), the ECM is apparently also serving as a protective barrier and transport modulator or “buffer.” The somatic cells in the periphery seem to be the only cells strongly affected by the inhibitor in the intact colony.

Results: Particle Imaging Velocimetry (PIV)

We turn now to direct visualizations of the flow fields around *V. carteri*. The power of this method for acquiring detailed information about flow fields is demonstrated in Fig. 5, a view along the colony axis. Fluid circulates around the colony equator in a manner directly related to the characteristic rolling motions *Volvox* displays as it swims. Returning to the flow geometry of Fig. 3, Fig. 6*a* shows a typical example of a complete flow field, from which it is apparent that the flow extends over many colony diameters, and that the maximum velocity is near the equator. The velocity slice in Fig. 6*b* reveals a peak of $\approx 800 \mu\text{m/s}$ for a colony of radius $200 \mu\text{m}$. Collecting together results at the four life cycle stages, Fig. 7*a* shows that the maximum fluid velocity

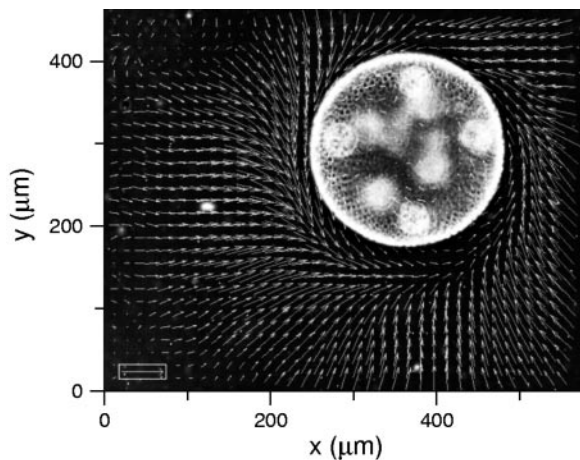


Fig. 5. PIV flow field around a sessile *V. carteri* colony. Taken in a plane perpendicular to the colony axis, this top view shows swirling flows around equator of colony. Bright circles in the superimposed negative image are developing daughter colonies.

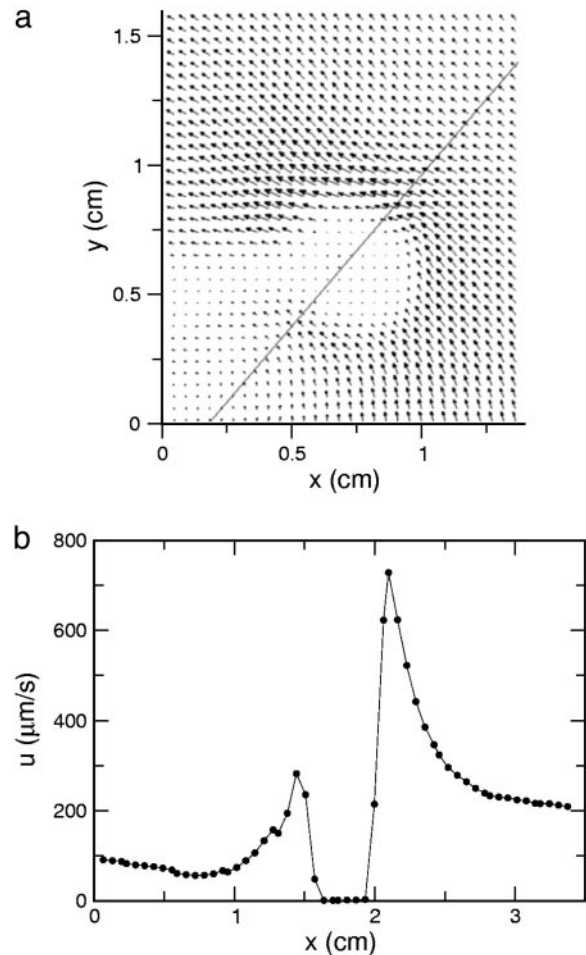


Fig. 6. Results from PIV. (a) Fluid velocity field surrounding an immobilized colony of *V. carteri*, with equatorial slice indicated. (b) Fluid velocity along equatorial slice.

as a function of time is nonmonotonic, peaking strongly at the division stage. Although the colony diameter increases only $\approx 30\%$ from the hatch to division stage, the fluid velocity nearly doubles. High-speed imaging of the flagella in both stages showed progressive elongation from $9.7 \pm 0.2 \mu\text{m}$ for recently hatched to $12.4 \pm 0.4 \mu\text{m}$ at the division stage, and on to $13.4 \pm 0.4 \mu\text{m}$ by stage IV. The flagellar beating rates were found to have a slow decline during the whole of the life cycle, from $\approx 22 \text{ Hz}$ when cells have just hatched to $\approx 17 \text{ Hz}$ at the pre-hatch stage (Fig. 7*b*). The hydrodynamic mechanism responsible for the marked increase in fluid velocity near stage II is not clear, especially because neither the flagellar length nor beating frequency show a dramatic change there. It is possible that the efficiency of the flagella in producing the streaming motion is a sensitive function of the inter-somatic cell distance.

Using the colony diameter as the characteristic length scale, and $D = 10^{-5} \text{ cm}^2/\text{s}$ as a representative diffusion constant for small solutes, Fig. 8 shows the Peclet number Pe derived from the measured maximum velocities. These exceed unity by two orders of magnitude during the entire life cycle; there is no doubt that advective transport dominates diffusion. Superimposed on the gradual increase in Pe due to colony growth is a spike at the division stage, so the advective transport rate is similarly enhanced.

These flow fields, driven by the surface-mounted flagella, also have remarkable near-field properties. Viewed at higher mag-

of the form $d = d_0 + \sum_i a_i v_i + \sum_{ij} b_{ij} v_i v_j$ was performed by using indicator (dummy) variables $v_i = 0,1$ to take the nominal factors into account (medium, deflagellation, broken colony, and inhibitor treatments). Reported statistical variations are standard errors. Dummy variables allow analyses of categorical variables by comparison of several regression equations originating from a single multiple regression. JUMP software (SAS Institute, Cary, NC) was used for the analysis.

In complementary experiments, we measured flagellar-driven flows (35, 36) around *V. carteri* using PIV. The life cycle was sampled in 2-h windows beginning at each of four stages: I, hour 1 (“growth”); II, hour 9 (“division”); III, hour 25 (“daughter”); IV, hour 33 (“prehatch”). Effects associated with colony translocation were eliminated by holding colonies fixed by micropipette aspiration (Fig. 3). Elsewhere (M. B. Short, C.A.S., S. Ganguly, T. R. Powers, J.O.K., and R.E.G., unpublished work), we show in the context of a detailed model of the flow field generated by the somatic cells’ flagella that there are only minor differences in the scales of velocity at the surface of immobilized cells and those that are swimming. Micropipettes with diameters of $\approx 10 \mu\text{m}$ were produced with a pipette puller (P-87, Sutter Instruments, Novato, CA). Suction was applied through the gentle withdrawal of a gas-tight syringe attached to the pipette with flexible tubing. The flow past a colony has two stagnation

points, and the germ cells lie in the posterior half of the colony near one of them (Fig. 3). To measure the maximum fluid velocity along the colony surface without interference from the micropipette, the aspiration point was chosen midway between the posterior stagnation point and the equator. An equatorial slice yields the peak velocity. Because the microscope depth of field is small relative to the colony diameter, flow fields can be measured at a range of positions through the depth of the colony. Results reported represent those from the midsection.

Flows were imaged with microspheres (Molecular Probes, F8825 carboxylate modified, $1.0 \mu\text{m}$, Nile red), viewed by using laser epifluorescence (80 mW, 532 nm), or by dark-field illumination. A typical objective magnification was $\times 4$ on an inverted microscope (Diaphot 200, Nikon). Movies acquired with an analog charge-coupled device camera (SSC-M374, Sony; 480×640 pixels) consisted of $\approx 1,000$ images taken at ≈ 30 frames per s, averaged over ≥ 200 frames. Commercial PIV software (Dantec Dynamics, Skovlunde, Denmark) was used. Flagellar lengths and beating rates were determined at higher magnification by using a high-speed camera (ES-310T, Kodak).

We thank T. Huxman and A. M. Nedelcu for important discussions and L. Cisneros, C. Dombrowski, and C. Smillie for experimental assistance. This work was supported in part by National Science Foundation Grants DEB-0075296 and PHY-0551742.

- Enquist, B. J. & Niklas, K. J. (2001) *Nature* **410**, 655–660.
- Niklas, K. J. & Enquist, B. J. (2001) *Proc. Natl. Acad. Sci. USA* **98**, 2922–2927.
- West, G. B., Brown, J. H. & Enquist, B. J. (1999) *Science* **284**, 1677–1679.
- West, G. B., Brown, J. H. & Enquist, B. J. (1997) *Science* **276**, 122–126.
- Maynard Smith, J. & Száthmary, E. (1995) *The Major Transitions in Evolution* (Freeman, San Francisco).
- Michod, R. E. (1999) *Evolutionary Transitions in Fitness and Individuality* (Princeton Univ. Press, Princeton).
- Niklas, K. J. (2000) *Ann. Bot.* **85**, 411–438.
- Schulz, H. N. & Jørgensen, B. B. (2001) *Annu. Rev. Microbiol.* **55**, 105–137.
- Kirk, D. L. (1998) *Volvox: Molecular-Genetic Origins of Multicellularity and Cellular Differentiation* (Cambridge Univ. Press, Cambridge, U.K.).
- Koufopanou, V. (1994) *Am. Nat.* **143**, 907–931.
- Nozaki, H. (2003) *Biologia* **58**, 425–431.
- Coleman, A. W. (1999) *Proc. Natl. Acad. Sci. USA* **96**, 13892–13897.
- Desnitski, A. G. (1995) *Eur. J. Protistol.* **31**, 241–247.
- Reynolds, C. S. (1984) *The Ecology of Freshwater Phytoplankton* (Cambridge Univ. Press, Cambridge, U.K.).
- Solari, C. A., Kessler, J. O. & Michod, R. E. (2005) *Am. Nat.*, in press.
- Ibañez-Tallon, I., Heintz, N. & Omran, H. (2003) *Hum. Mol. Genet.* **12**, R27–R35.
- Pazour, G. J., Agrin, N., Leszyk, J. & Witman, G. B. (2005) *J. Cell Biol.* **170**, 103–113.
- Nonaka, S., Shiratori, H., Saijoh, Y. & Hirokawa, N. (2002) *Nature* **418**, 96–99.
- Cartwright, J. H. E., Piro, O. & Tuval, I. (2004) *Proc. Natl. Acad. Sci. USA* **101**, 7234–7239.
- Darnton, N., Turner, L., Breuer, K. & Berg, H. C. (2004) *Biophys. J.* **86**, 1863–1870.
- Dombrowski, C., Cisneros, L., Chatkaew, S., Goldstein, R. E. & Kessler, J. O. (2004) *Phys. Rev. Lett.* **93**, 098103.
- Tuval, I., Cisneros, L., Dombrowski, C., Wolgemuth, C. W., Kessler, J. O. & Goldstein, R. E. (2005) *Proc. Natl. Acad. Sci. USA* **102**, 2277–2282.
- Wu, X.-L. & Libchaber, A. (2000) *Phys. Rev. Lett.* **84**, 3017–3020.
- Guyon, E., Hulin, J. P., Petit, L. & Mitescu, C. D. (2001) *Physical Hydrodynamics* (Oxford Univ. Press, New York).
- Berg, H. C. & Purcell, E. M. (1977) *Biophys. J.* **20**, 193–219.
- Keller, E. F. & Segel, L. A. (1971) *J. Theor. Biol.* **30**, 225–234.
- Orme, B. A. A., Blake, J. R. & Otto, S. R. (2003) *J. Fluid Mech.* **475**, 333–355.
- Bell, G. (1985) in *The Origin and Evolution of Sex*, eds Halvorson, H. O. & Monroy, A. (Liss, New York), pp. 221–256.
- Koufopanou, V. & Bell, G. (1993) *Proc. R. Soc. London Ser. B* **254**, 107–113.
- Niklas, K. J. (1994) *Plant Allometry: The Scaling of Form and Process* (Univ. Chicago Press, Chicago).
- Solari, C. A. (2005) Ph.D. dissertation (Univ. of Arizona, Tucson).
- Sommer, U. & Gliwicz, Z. M. (1986) *Limnol. Oceanogr.* **31**, 650–653.
- Kirk, D. L. & Kirk, M. M. (1983) *Dev. Biol.* **96**, 493–506.
- Rosenbaum, J. L., Moulder, J. E. & Ringo, D. L. (1969) *J. Cell Biol.* **41**, 600–619.
- Hand, W. G. & Haupt, W. (1972) *J. Protozool.* **18**, 361–364.
- Hiatt, J. D. F. & Hand, W. G. (1972) *J. Protozool.* **19**, 488–489.